Organ-level phenotyping extraction of potted wheat key growth period based on point cloud

Xu Zhang[1†], Weiting Pan[1†], Deran Cheng[1], Chunying Wang[1,2], Haixia Yu[3], Ping Liu[1,2*], Xiang Li[3*]

(1. *College of Mechanical and Electronic Engineering, Shandong Agricultural University, Tai'an 271018, Shandong, China*;
2. *Shandong Engineering Research Center of Agricultural Equipment Intelligentization, Shandong Agricultural University, Tai'an 271018, Shandong, China*;
3. *State Key Laboratory of Wheat Improvement, Shandong Agricultural University, Tai'an 271018, Shandong, China*)

Abstract: Genotyping and phenotyping are critical for wheat breeding, with accurate phenotypic acquisition from potted wheat using 3D point cloud technology essential to overcoming bottlenecks from slow, inefficient processes. This study focuses on developing methods for accurate organ-level phenotypic data extraction from potted wheat plants using 3D point cloud techniques. The study exploited a multi-view acquisition system to construct point cloud datasets for wheat key growth stages and trained a network. Semantic (organ classification) and instance (organ segmentation) segmentation were performed on potted wheat to extract organ-level wheat point clouds. However, the imbalance in point cloud proportions among different wheat organs caused low semantic segmentation accuracy, and the interference from awns caused significant distortion in ear point clouds after instance segmentation. To address these issues, a class-related sampling strategy based on RandLA-Net was proposed, which balances various organ point clouds through a class-related sampling strategy. In addition, a geometric symmetry-based point cloud completion method was introduced to replenish the distorted wheat ear point cloud. Based on the segmented organ point clouds, phenotypic parameters were obtained using minimum bounding box and quadratic surface fitting methods. The results showed that semantic segmentation accuracy improved by 13.6% through class point balancing, and the determination coefficient for the extracted ear volume increased by 10.2% after point cloud completion. The obtained phenotypic parameters showed a strong correlation with manual measurements (determination coefficients ranging from 0.7737 to 0.9552). These phenotype acquisition methods provide accurate and practical phenotypic acquisition, supporting wheat optimization and superior gene screening.

Keywords: wheat, key growth period, 3D point cloud, organ segmentation, phenotypic analysis
DOI: 10.25165/j.ijabe.20261903.10466

Citation: Zhang X, Pan W T, Cheng D R, Wang C Y, Yu H X, Liu P, et al. Organ-level phenotyping extraction of potted wheat key growth period based on point cloud. Int J Agric & Biol Eng, 2026; 19(3): 243–255.

1 Introduction

Wheat, as one of the world's most important food crops, requires phenotyping for future varietal improvement[1-3]. Over the past decade, next-generation sequencing technologies have enabled breeders to genotype wheat rapidly and cost-effectively, screening for high-yield and stress-resistant genes[4,5]. However, the full potential of crop breeding can only be realized by integrating genomic data with high-quality phenotypic data[6]. In traditional wheat breeding programs, researchers typically grow large numbers of potted plants in greenhouses and rely on manual measurements and visual observations to characterize phenotypic traits for variety evaluation. These methods, however, are time-consuming and labor-intensive, requiring substantial human effort—especially when applied to large sample sizes. Therefore, the development of precise, efficient, and non-invasive methods for phenotypic data acquisition and processing is crucial for the in-depth analysis of wheat phenotypes and subsequent breeding efforts[7,8].

In recent years, advancements in imaging technologies and computational capabilities have enabled image-based phenotyping to non-invasively extract a large number of morphological traits within a short period and allow repeated quantification of the same traits throughout the wheat lifecycle[9-13]. However, due to the lack of depth information, these methods are easily affected by crop occlusion, overlap, and shooting angles[14,15]. The advent of 3D point clouds offers new possibilities for breeders to continuously monitor and quantify wheat growth and development[16,17]. Gu et al.[18] employed UAV-mounted LiDAR to capture 3D point clouds of wheat populations for assessing spatial distribution, while Li et al.[19] utilized a RGB camera-equipped UAV with five-direction oblique photography to reconstruct 3D point clouds for estimating plant height and biomass. Similarly, Zou et al.[20] achieved wheat ear counting and density estimation using point clouds acquired via a vehicle-mounted binocular camera system.

Alongside point cloud acquisition from crop canopies and populations, accurate organ-level segmentation is crucial for measuring phenotypic traits like leaf length and width, and has been

Received date: 2026-03-02 **Accepted date:** 2026-04-15
Biographies: Xu Zhang, PhD, research interest: crop phenotyping robots, Email: tjy46038@163.com; **Weiting Pan**, MS, research interest: 3D reconstruction and segmentation algorithm of wheat, Email: 17861501669@163.com; **Deran Cheng**, MS, research interest: 3D reconstruction and segmentation algorithm of crop, Email: chengderan123@163.com; **Chunying Wang**, Professor, research interest: image processing for wheat phenotyping, Email: wcychunying@126.com; **Haixia Yu**, Professor, research interest: mechanisms and applications of high and stable crop yield, Email: yuhaixia66@126.com.
†These authors have contributed equally to this work and share first authorship.
***Corresponding author: Ping Liu**, Professor, research interest: key technology of crop phenotyping robots. College of Mechanical and Electronic Engineering, Shandong Agricultural University, Tai'an 271018, Shandong, China. Tel: +86-18660888134, Email: liupingsdau@126.com; **Xiang Li**, Professor, research interest: mechanisms and applications of high and stable crop yield. State Key Laboratory of Wheat Improvement, Shandong Agricultural University, Tai'an 271018, China. Tel: +86-18660888290, Email: lixiang@sdau.edu.cn.

widely studied[21-23]. Traditional methods primarily target plants with specific morphologies, using topological and morphological features as prior knowledge to create manual segmentation features[24,25]. These methods do not require data annotation and can yield effective results for plants with certain morphologies. However, their generality and accuracy pose significant challenges when applied to complex and variable morphologies such as those of wheat and sorghum. Deep learning methods employ data-driven strategies to directly learn point cloud feature extraction and combination schemes, offering higher segmentation accuracy and generality compared to traditional methods[26-28]. Currently, many studies use deep learning networks to abstract point cloud features for semantic and instance segmentation of crop organs[29,30]. For instance, Patel et al. used four-point cloud deep learning models—PointNet, PointNet++, PointCNN, and dynamic graph CNN (Convolutional Neural Networks)—to segment sorghum into stems, leaves, and panicles, finding that the PointNet++ model yielded the best results[31]. Gong et al.[32] designed the Panicle-3D model, a 3D point cloud CNN that targets multi-scale features of crop organs, combining the PointConv structure and long-short jumps to accelerate network convergence and reduce feature loss during point down-sampling. Li et al.[33] developed a plant point cloud segmentation technique, DeepSeg3DMaize, which integrates data acquisition and deep learning to perform instance segmentation of stems and organs using PointNet.

While these studies have provided a theoretical and methodological foundation for crop phenotyping, research specifically focused on the acquisition and analysis of organ-level phenotypic parameters from wheat point clouds remains limited. This is primarily due to severe leaf overlap, numerous tillers, and significant regional variation in organ point clouds within the plants[34]. Existing plant point cloud segmentation methods often lack sufficient accuracy when dealing with structurally complex and densely occluded plants, struggling to distinguish tightly arranged plant parts—particularly during instance segmentation, where label confusion frequently occurs. Therefore, there is a need to develop a targeted approach capable of achieving precise segmentation of wheat point clouds across different growth stages. Addressing these issues, the study focuses on wheat from the three-leaf stage to the heading stage, conducting organ-level phenotypic analysis based on point clouds during key growth periods. The main contributions of this research are as follows: constructed a wheat point cloud dataset for organ segmentation; proposed a wheat point cloud organ semantic segmentation algorithm based on class-related sampling strategy to improve segmentation accuracy; developed a Density-Based Spatial Clustering of Applications with Noise (DBSCAN) method based on the maximum distance between k-nearest points for instance segmentation of wheat ear point cloud instances, using geometric symmetry-based point completion method to supplement point cloud loss caused by awn filtering; proposed a skeleton extraction method based on the Laplacian contraction operator to achieve instance segmentation of wheat stems and leaves, obtaining leaf surface equations based on continuous local quadratic surface fitting to extract leaf-related phenotypic parameters (leaf length, leaf curvature).

2 Materials and methods

2.1 Wheat point cloud dataset construction

2.1.1 Wheat point cloud data acquisition

From April 2022 to November 2023, the study cultivated wheat in a controlled environment chamber at the National Key Laboratory of Wheat Improvement at Shandong Agricultural University (36°11′39.588″N, 117°7′10.848″E) and captured images for analysis. The experimental wheat was the inbred line Fielder, grown in 5.7-liter pots filled with PINDSTRUP peat soil (Sphagnum peat, mixed with a certain proportion of vermiculite and perlite). The soil had a maximum water content of approximately 40%. The controlled environment chamber was maintained at a constant temperature of 24°C±1°C, with relative humidity at 40%, a light cycle of 16 hours of illumination (6:00 am to 10:00 pm), 8 hours of darkness, and an indoor light intensity of 30klux. This study utilized a multi-view acquisition device for potted plants to continuously capture multi-view images of 125 wheat plants from the three-leaf stage to the heading stage in a controlled environment chamber (Figure 1a). The captured images were processed using COLMAP software (Girardeau-Montaut, 2015) through point cloud reconstruction methods, including structure-from-motion (SfM) for sparse reconstruction and multi-view stereo (MVS) for dense reconstruction, resulting in a total of 500 raw point clouds across four growth stages (Figure 1b).

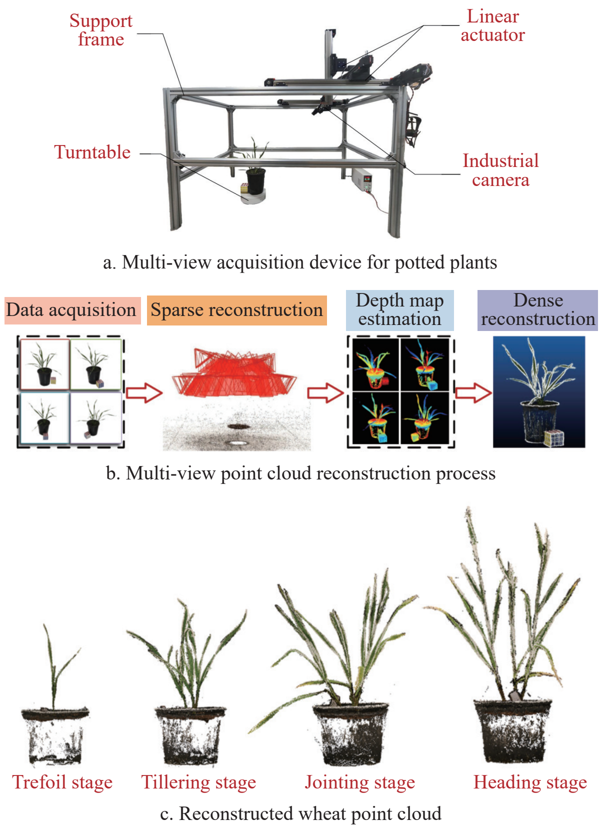

a. Multi-view acquisition device for potted plants

b. Multi-view point cloud reconstruction process

c. Reconstructed wheat point cloud

Figure 1 Multi-view acquisition and 3D reconstruction of wheat plant point clouds

The raw point cloud data contained portions of the surrounding environment as well as the calibration object (a Rubik's cube). After spatial scale calibration and center alignment, the data were registered to the XY plane and scaled to real-world dimensions, with the center of the plant point cloud positioned near the z-axis. The procedure for acquiring multi-view images of wheat plants was as follows: (1) White background panels were vertically installed on three inner sides of the acquisition device. A wheat plant and a calibration object (a Rubik's cube) were placed on a turntable capable of rotating at fixed intervals. (2) The linear actuator was adjusted to position the camera at its lowest point (500 mm above the base of the device), and the gimbal connected to the camera was oriented to face the wheat plant directly. (3) The camera was set to capture multi-view images at fixed time intervals (2 s between shots), with an angular separation of 8 degrees between consecutive images. (4) Depending on the plant height at different growth stages, the camera height and viewing angle were adjusted (600 mm for the three-leaf stage, 650 mm for the tillering stage, 700 mm for the jointing stage, and 800 mm for the heading stage above the base of the device). Step (3) was repeated to capture high-angle multi-view images. Ultimately, 90 images were acquired per plant in each session for point cloud reconstruction.

2.1.2 Dataset construction

Due to various factors including environmental conditions, imaging equipment, and indoor lighting, point cloud data often contained noise at different scales, such as large-scale noise from the reference cube and small-scale noise around the wheat plants. The large-scale noise was generally uniformly distributed, had a significant volume, and was aligned parallel or perpendicular to the horizontal plane. This noise was removed using a pass-through filter in CloudCompare by selecting the specific region. Small-scale noise, which was scattered and had a lower point density, was primarily concentrated around the wheat plants. To address this, the study employed the Statistical Outlier Removal (SOR) algorithm to eliminate small-scale noise. This algorithm identified noise points based on the statistical deviation of data points from their neighbors. Additionally, limitations of the imaging equipment and environmental conditions often resulted in uneven density in the reconstructed point cloud data, complicating data processing. To effectively reduce computational complexity, decrease data storage and transmission overhead, and preserve critical features of the point cloud, the study used voxel grid filtering in CloudCompare. The LeafSize was set to 0.005 to reduce the number of points in the point cloud. The point cloud filtering and down-sampling results are shown in Figure 2.

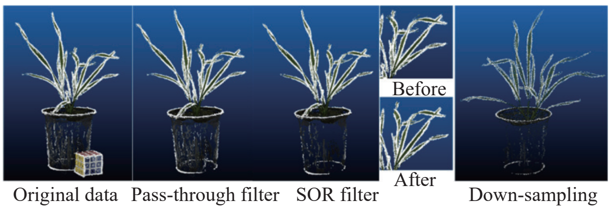

Figure 2 Illustration of the preprocessing effects on wheat point clouds

Depending on the segmentation objectives, this study utilized CloudCompare software to perform data annotation and create two distinct segmentation datasets: (1) Organ Classification Dataset: A unified segmentation protocol was applied to classify point clouds into four categories: leaf, stem, ear, and non-plant elements, with corresponding semantic labels assigned (Figure 3a). This dataset aims to segment individual wheat plants into four components: stem, leaf, ear, and non-plant parts. This segmentation facilitates subsequent instance segmentation of organs and supports the extraction of phenotypic parameters such as plant height and compactness. Furthermore, to analyze growth dynamics of individual plants, point clouds obtained from the same plant across different time points were grouped and named according to the acquisition date. (2) Organ Instance Segmentation Dataset: Within the same wheat point cloud, points originating from different instances were assigned unique identifiers as instance labels (Figure 3b). The objective of this dataset is to segment wheat organs into individual leaves, stems, and ears. Such detailed segmentation enables the extraction of organ-level phenotypic parameters, including leaf area, ear volume, and stem tilt angle. For each segmented dataset, the annotated point cloud data were partitioned into training, validation, and test subsets at a ratio of 70%, 20%, and 10%, respectively.

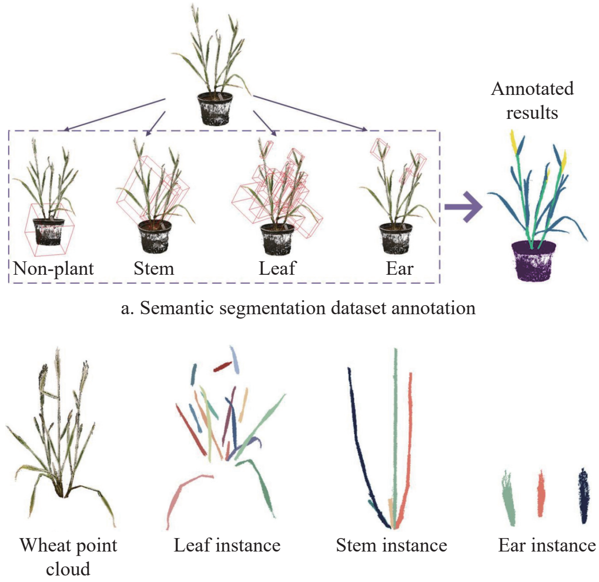

a. Semantic segmentation dataset annotation

b. Instance segmentation dataset annotation

Figure 3 Annotation of the wheat organ segmentation dataset

2.2 Point cloud segmentation of wheat organs

2.2.1 Semantic segmentation of wheat organs based on RandLA-Net and class-point balancing algorithm

Utilizing deep learning for wheat organ point cloud segmentation was fundamental for the subsequent segmentation of individual ears, leaves, and stems. However, the unordered, sparse, and unstructured nature of point clouds presented significant challenges[35]. To accurately obtain individual wheat organ point clouds, the study used the RandLA-Net point cloud segmentation network[36] as the baseline network and employed a class-related strategy to balance the proportion of each class in the point cloud, as shown in Figure 4a.

First, the point cloud was fed into a shared multilayer perceptron (MLP) to extract per-point features. This was followed by four encoder-decoder layers to learn the features of each point. Finally, three fully connected (FC) layers and a dropout layer were used to predict the semantic labels of each point. The encoder-decoder layers incorporated a local feature aggregation module to retain significant features of the point cloud, balancing segmentation efficiency and effectiveness. This module effectively preserved complex local structures by considering adjacent geometries and significantly increasing the receptive field. However, not all plant and non-plant parts had equal data volumes in the point cloud. As illustrated in Figure 4b, the segmentation performance for minority classes was significantly lower than for majority classes, impacting the overall segmentation quality. To address this issue, the study designed a class-related sampling strategy to combat class imbalance.

The class-related sampling strategy balanced class points by dividing the original point cloud of the training set into blocks [37], which involved two main steps. First, a predefined number of anchor points were sampled from the point cloud for each class. Second, neighboring points were added to the anchor point set based on k-nearest neighbor (k-NN) search, forming new data from the selected points. The number of anchor points for each class was determined based on the inverse of the original class point proportion, as shown in Equation (1):

$$a_c = \frac{1 - \dfrac{n_c}{n}}{\sum_{i=1}^{C}\left(1 - \dfrac{n_i}{n}\right)} \times 100 \tag{1}$$

where, a_c represented the number of anchor points for a class; n_c represented the number of points for a class; n represented the total number of points in the point cloud; C represented the number of classes. The balanced point cloud was employed as a novel training set to train the segmentation network.

The number of points from different classes within the point block depended on the size of the target class and the value of k. In the study, k values were selected as 512, 1024, 2048, 4096, and 8192 to balance the number of points in each class. The class proportions after balancing are shown in Figures 4b and 4c. The balanced data was then used to train and test the segmentation network, resulting in relatively optimal class balance and point cloud classification performance.

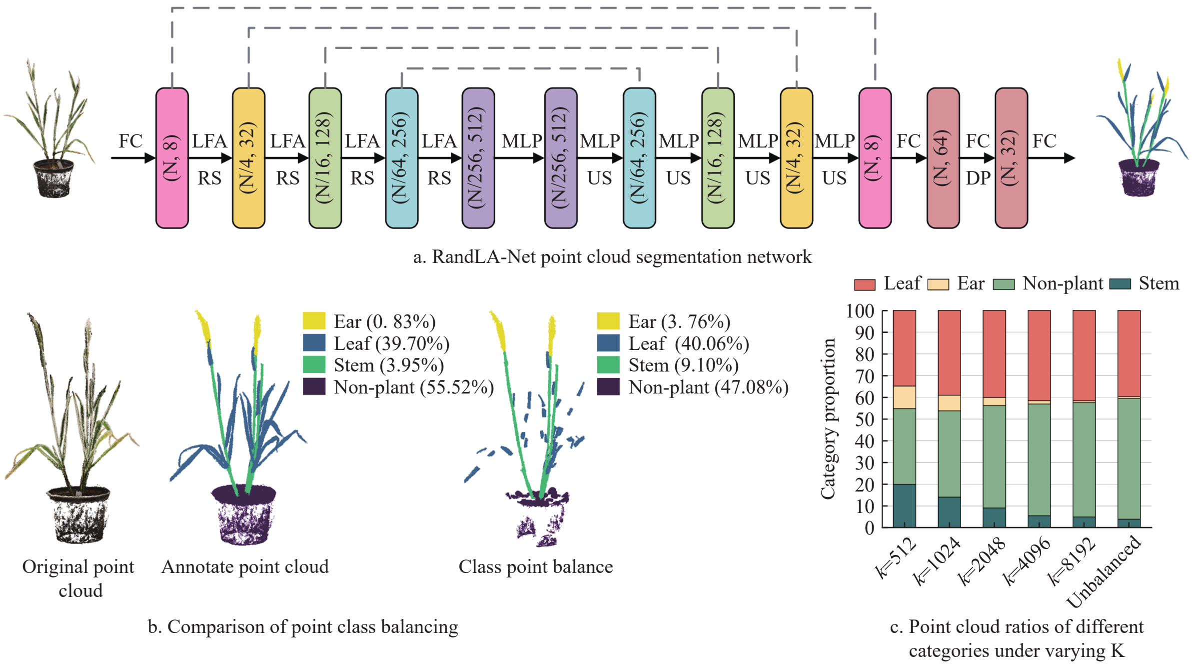

Figure 4 Semantic segmentation of wheat organs based on RandLA-Net network and class point balancing algorithm

2.2.2 Wheat ear instance segmentation

To further obtain phenotype at the wheat organ level, the study proposed a DBSCAN-based method that leveraged the maximum distance among k-nearest neighbors to adaptively adjust the search radius. This approach enabled the automatic and precise instance segmentation of wheat ears in the point cloud data. The DBSCAN method was effective for detecting clusters of arbitrary shapes in any dimensional space, making it highly suitable for segmenting wheat ears, even when parts of the point cloud were missing. Additionally, unlike K-means and other clustering methods, DBSCAN did not require a predefined number of clusters.

The DBSCAN method required at least two parameters: the proximate points (k_1) and the search radius ε. Based on the inherent properties of the point cloud data, the study estimated the parameter ε using the maximum distance among k-nearest neighbors.

To further enable organ-level phenotyping of wheat, this study proposes a DBSCAN-based method that adaptively determines the search radius based on the maximum distance among k-nearest neighbors, thereby achieving accurate and automatic instance segmentation of wheat ears from point cloud data. DBSCAN is effective for detecting clusters of arbitrary shapes in spaces of any dimensionality and is well suited for wheat ear segmentation even in cases where the point cloud is incomplete. Moreover, unlike K-means and other clustering methods, DBSCAN does not require a predefined search radius.

The DBSCAN algorithm requires at least two parameters: the number of neighboring points k_1 and the search radius ε. The clustering procedure is as follows: (1) For each point p_i, the number of points within its ε-neighborhood is counted. If this number is greater than or equal to k_1, the point is marked as a core point; (2) For each core point, all points within its ε-neighborhood (including non-core points) are assigned to the same cluster, and the neighborhood points of other core points within this region are recursively incorporated into the same cluster; (3) Points that are not density-reachable from any core point are labeled as noise and are excluded from clustering.

As shown in Figure 5, with a search radius ε and k_1=4, points p_2, p_3, and p_8 are identified as core points. Since p_3 lies within the ε-neighborhood of p_2, both p_2 and p_3, along with all points in their respective neighborhoods, are assigned to the same cluster. Points p_{11} and p_{12} are neither core points nor lie within the ε-neighborhood of any core point; they are therefore treated as noise.

The above analysis indicates that the search radius ε plays a critical role in determining the clustering outcome. Due to the influence of awns, the point cloud of wheat ears is often non-uniformly distributed and partially incomplete. Consequently, points at the ear boundaries can easily be misclassified as noise and excluded from clustering. To address this issue, this study proposes an adaptive method to determine ε based on the intrinsic properties of the ear point cloud, thereby improving the accuracy of ear segmentation.

For any point p_i in the ear point set $P\{p_1, p_2 ... p_i ... p_n\}$, its k_1-nearest neighbors (with k_1=10 in this study) are identified to form a point set $Q\{q_1, q_2 ... q_k\}$. The maximum distance from p_i to the points in Q is then calculated as Equation 2:

$$d_{\max i} = \max_{1 \le j \le k_1} d_{ij} \tag{2}$$

where, $d_{\max i}$ denotes the farthest distance between p_i and its k_1-nearest neighbors; and d_{ij} represents the distance between point p_i and any point q_1 in the point set Q.

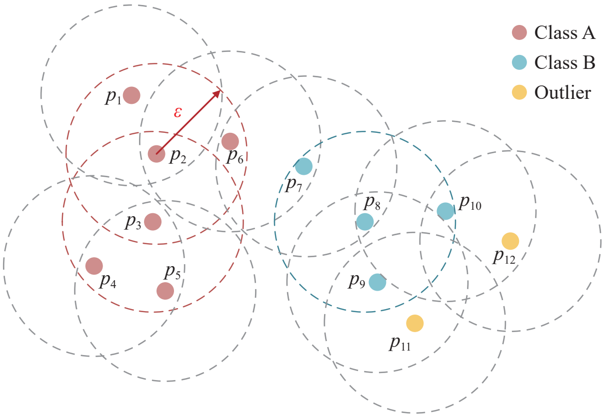

Figure 5 DBSCAN clustering process

This operation is repeated for all points in $P\{p_1, p_2 \ldots p_i \ldots p_n\}$, and the overall maximum distance among the k_1-nearest neighbors across the entire point set is defined as Equation 3:

$$D_k = \max_{1 \le i \le n} d_{\max i} \tag{3}$$

In this study, the search radius ε for the DBSCAN clustering algorithm is adaptively estimated using the k-nearest neighbors' approach, with ε set to D_k.

2.2.3 Wheat stem and leaf instance segmentation

Due to the significant overlap between wheat stems and leaves and their similar morphology, segmenting the wheat stem point cloud was challenging. The study proposed a curve skeleton extraction and stem-leaf segmentation method based on Laplacian contraction, utilizing the single-stem point clouds and leaf point clouds from organ segmentation and considering the structural characteristics of wheat stems and leaves. This method integrated the characteristics of wheat stem-leaf structures and aimed to handle discrete geometric data through local Delaunay triangulation and topological refinement. It also performed topology-driven repair of the acquired point cloud, particularly effective in scenarios with substantial data loss, to obtain a more realistic and efficient point cloud skeleton.

For a given point cloud $P = \{p_1 \ldots p_i \ldots p_n\}$, the process began by shrinking it into a zero-volume point set C. Subsequently, a subset of C was sampled using the farthest point sampling strategy to construct a skeleton graph G. Redundant edges in the skeleton graph G were removed through edge collapse operations to obtain the skeleton T. Finally, to confine the skeleton T within the point cloud P as closely as possible, each vertex of T was adjusted to the center of the local neighborhood of the point cloud. As demonstrated during the tillering and jointing stages of wheat growth, the effectiveness of stem and leaf skeleton extraction is illustrated in Figures 6c and 6d.

Based on the acquired associated point set, the point cloud was decomposed into skeletons and segmented into single leaf and stem point clouds to achieve instance segmentation of wheat stem and leaf organs, as depicted in Figures 6e and 6f. To address mis-segmentation issues during this process, a distance constraint on the point cloud within the associated point set was imposed to achieve more precise stem-leaf instance segmentation.

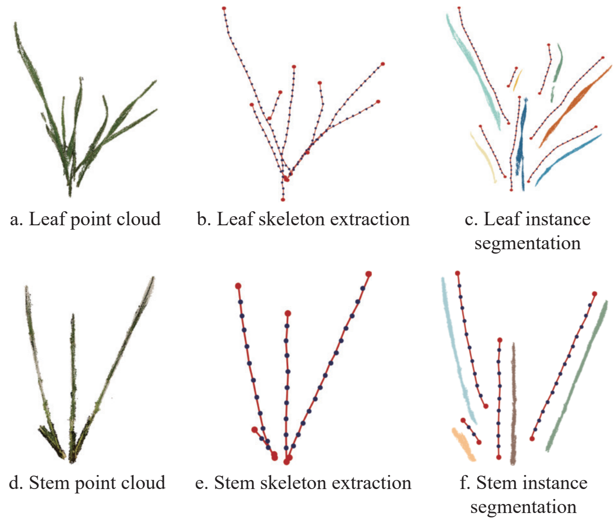

a. Leaf point cloud b. Leaf skeleton extraction c. Leaf instance segmentation

d. Stem point cloud e. Stem skeleton extraction f. Stem instance segmentation

Figure 6 Extraction and segmentation of wheat stem and leaf skeleton based on Laplacian contraction

2.3 Wheat phenotype acquisition

2.3.1 Phenotype acquisition of wheat plants

At the whole-plant scale of wheat, plant height and plant compactness were two key phenotypic parameters critical for evaluating wheat growth status and light utilization efficiency. In the study, wheat plant height was obtained using the method of minimum bounding box, while plant compactness was estimated by calculating the ratio of the projected area of the wheat plant point cloud to its convex hull volume (Figure 7). The convex hull of a point cloud refers to the smallest convex set that contains all points. The projection plane is defined as the lowest plane of the plant point cloud, whose general form can be derived from the vertex coordinates of the minimum bounding box and expressed as Equation 4:

$$Ax + By + Cz + D = 0 \tag{4}$$

For any point $p_o(x_o, y_o, z_o)$ in the plant point cloud outside the plane, its projection onto the plane must satisfy the vertical constraint condition, that is:

$$y_p = \frac{B}{A}\left(x_p - x_o\right) + y_o \tag{5}$$

$$z_p = \frac{C}{A}\left(x_p - x_o\right) + z_o \tag{6}$$

where, x_p, y_p, and z_p are the coordinates of the projection of point p_0 onto the plane.

Thus, the projected coordinates on the plane can be obtained as:

$$x_p = \frac{\left(B^2 + C^2\right) x_o - A\left(By_o + Cz_o + D\right)}{A^2 + B^2 + C^2} \tag{7}$$

$$y_p = \frac{\left(A^2 + C^2\right) y_o - B\left(Ax_o + Cz_o + D\right)}{A^2 + B^2 + C^2} \tag{8}$$

$$z_p = \frac{\left(A^2 + B^2\right) z_o - C\left(Ax_o + By_o + D\right)}{A^2 + B^2 + C^2} \tag{9}$$

The projected area of a point cloud is approximated by dividing the projected point cloud into grids and calculating the grid area.

2.3.2 Phenotypic acquisition of wheat ears

Anatomical analysis of wheat ear morphology was an effective strategy for detecting yield traits, as it positively reflected grain size and number, thereby indicating the yield of individual wheat plants[38]. Due to the issue of awns causing cluttered point clouds at the edges of wheat ears, the study first employed filtering to remove awn point clouds. However, filtering resulted in missing data in the wheat ear point clouds. Therefore, before extracting wheat ear phenotypic parameters (ear length, ear width, ear volume), the study utilized a geometric approach to supplement the point cloud based on the relatively symmetrical structural characteristics of the wheat ear, aiming to achieve a more complete point cloud. Specifically, the center axis of the wheat ear point cloud was fitted using the Random Sample Consensus (RANSAC) algorithm. The wheat ear point cloud was then sliced along the central axis direction (with a slice thickness set to 0.002 and a spacing of 0.002 between adjacent slices), as shown on the left side of Figure 8a. Each layer of the sliced point cloud was symmetrically constructed into a new wheat ear point cloud centered on the centroid, as shown on the right side of Figure 8a.

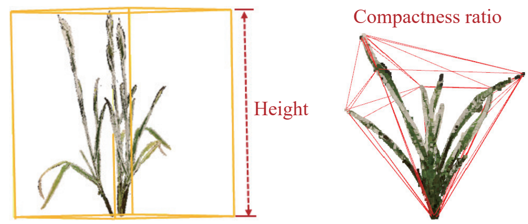

Figure 7 Wheat plant height and compactness acquisition

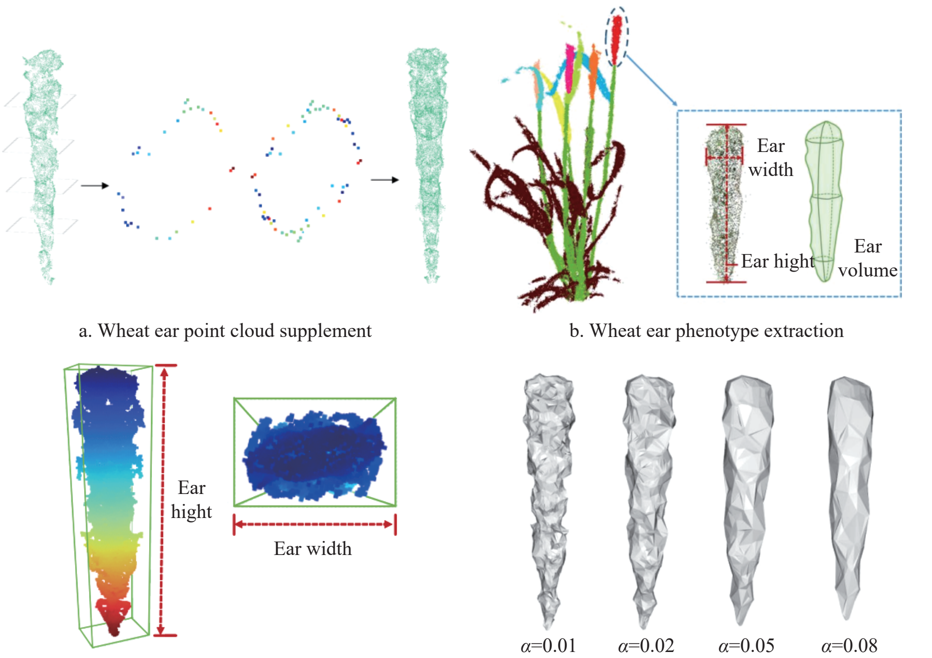

a. Wheat ear point cloud supplement

b. Wheat ear phenotype extraction

c. Ear length and width extraction

d. Wheat ear surface reconstruction with different α values

Figure 8 Supplementation of wheat ear point clouds based on geometric symmetry and calculation of ear phenotypes using the minimum bounding box

After supplementing the wheat ear point cloud, phenotypic parameters were extracted based on the morphological characteristics of the wheat ear. The ear length and width were obtained using the minimum bounding box method, while the ear volume was determined using the Alpha shapes surface reconstruction method, which converted the unstructured point cloud into a closed shape composed of triangular meshes (Figures 8b and 8c). The reconstruction effect was determined by setting different search radii for the outer contour (Figure 8d) (a radius too large lost the original structural features of the ear, while a radius too small was easily affected by missing point cloud data). The study set an optimal radius for wheat ear surface reconstruction.

2.3.3 Phenotypic acquisition of wheat stem and leaf

Leaves are the largest organs on the surface of wheat plants and are the primary sites for photosynthesis and respiration. Analyzing leaf phenotypic parameters (leaf length, leaf area, leaf curvature, and flag leaf inclination angle) is crucial for exploring their structural advantages[39]. Meanwhile, the degree of stem inclination determines the lodging resistance of the plant. The study used the method of quadratic surface fitting to calculate leaf curvature. Based on the extracted single leaf point cloud skeleton, the endpoint coordinates $p_1(x_1,y_1,z_1)$ and $p_2(x_2,y_2,z_2)$ of the leaf were determined. The distance along the fitted quadratic surface equation between points p_1 and p_2 represents the length of the leaf. Wheat flag leaves often exhibited a short and flat state. Based on this structural characteristic, the flag leaf inclination angle θ was determined in this study using the average unit normal vector $\check{n}$ of the leaf derived from its quadratic fitting surface, together with the stem direction vector $\check{S}$. Leaf area calculation adopted voxel grid to directly obtain the area of the discrete point cloud. In this process, each point in the point cloud was mapped to one or more voxels (cubic elements) in space, representing the point cloud data as a dense three-dimensional grid. The degree of stem inclination was determined by the ground normal vector $\check{n}$ and the stem direction vector $\check{S}$ (Figure 9).

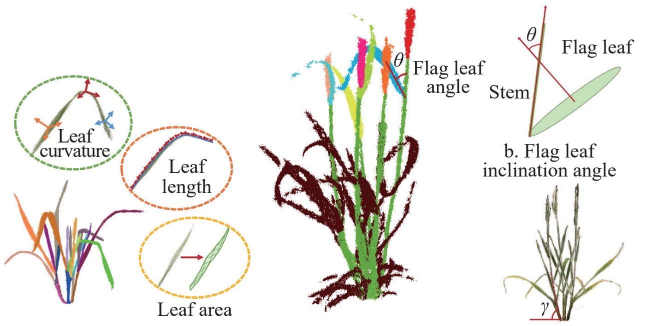

a. Schematic diagram of leaf phenotype

b. Flag leaf inclination angle

c. Stem inclination angle

Figure 9 Extraction of wheat organ phenotypes

3 Results

3.1 Semantic segmentation based on class-point balancing algorithm

To verify the segmentation performance of the organ segmentation network after class balancing, the study validated wheat point clouds at different growth stages. Wheat growth stages mainly included the three-leaf stage, tillering stage, jointing stage, and heading stage. Figure 10 shows the organ segmentation results of wheat point clouds at different growth stages under four class balancing states.

The results indicated that the RandLA-Net point cloud segmentation network exhibited severe mis-segmentation of wheat leaves, stems, and ears when class balancing was not performed. The primary reason was the significant imbalance in the proportions of different organ point clouds within the entire wheat point cloud, where the numbers of stem and ear point clouds were much lower compared to leaf and non-plant point clouds. After class balancing, the organ segmentation network showed significant improvements in correctly identifying point clouds. Compared to the unbalanced class point state, when balancing block sizes were set to K=1024, K=2048, K=4096, and K=8192, segmentation performance for leaf, stem, and ear point clouds all showed improvements (Figure 11a). Particularly, the segmentation performance improved most notably with a block size of K=2048, and segmentation performance between different classes became more balanced. Additionally, after balancing wheat point clouds with a block size of K=2048, the mean Intersection over Union (mIoU), average precision, and average accuracy of point cloud segmentation reached their highest levels, with relatively high average recall (Figure 11b).

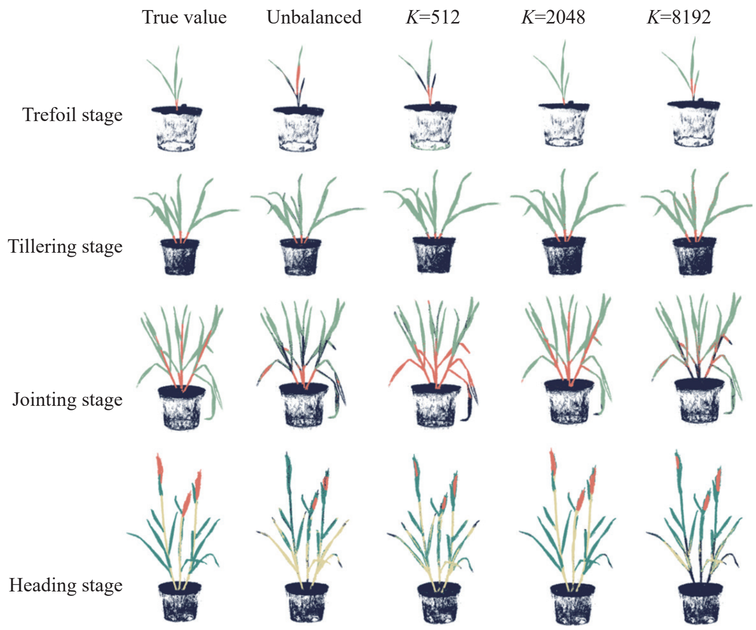

Figure 10 Diagram of wheat organ semantic segmentation based on the class point balance algorithm

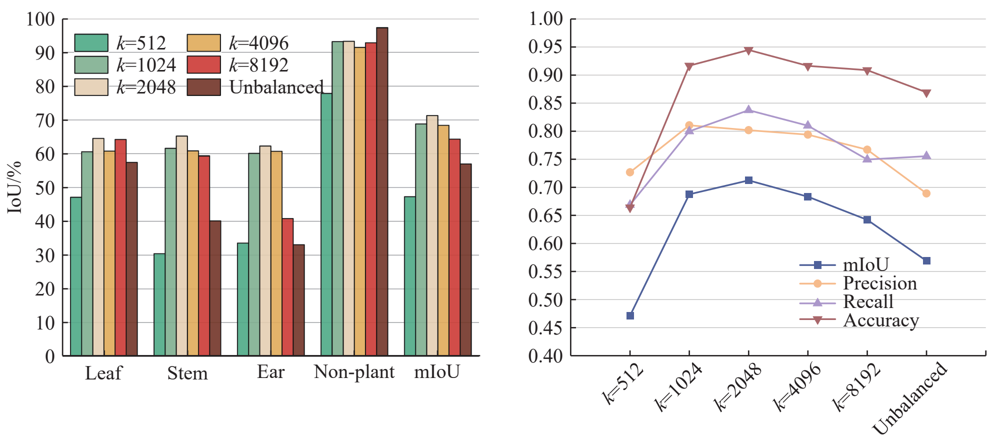

a. IoU values for organ segmentation with different k values

b. Wheat organs segmentation results under different point equilibria

Figure 11 Comparison of wheat organ point cloud segmentation results under different class-point balance states

In addition, four other network models—GMMConv[40], PointCNN[41], Kpconv[42], and FeaStConv[43]—were applied to train on the wheat dataset before and after class balancing, and were tested using the pre-balancing data. These models were configured and trained following the optimization parameters recommended in their respective official guidelines. All models were trained until the loss function showed minimal improvement. The semantic segmentation performance of these four models on the test set was then obtained and compared with RandLA-Net used in this study, as listed in Table 1. The results indicate that training with the class-balanced data significantly improves model performance. Furthermore, RandLA-Net demonstrates more balanced performance across different wheat organs for semantic segmentation compared to the other networks.

Table 1 Semantic segmentation results of wheat organ point clouds under different equilibrium states of class points

	Unbalanced					Balanced				
	mIoU	IoU_ non-plant	IoU_Leaf	IoU_Stem	IoU_Ear	mIoU	IoU_ non-plant	IoU_Leaf	IoU_Stem	IoU_Ear
GMMConv	0.6941	0.9892	0.8814	0.5089	0.3970	0.7893	0.8464	0.4733	0.5208	0.6467
PointCNN	0.5835	0.9745	0.7335	0.6260	0.0000	0.6066	0.9855	0.8662	0.2983	0.2762
Kpconv	0.4292	0.9838	0.5169	0.3576	0.3425	0.7067	0.9812	0.7815	0.4848	0.5793
FeaStConv	0.7135	0.9900	0.8882	0.5069	0.4687	0.8009	0.9873	0.8407	0.7066	0.5690
RandLA-Net	0.6695	0.9418	0.8642	0.3320	0.5398	0.7145	0.9236	0.6503	0.6678	0.6372

3.2 Wheat point cloud instance segmentation

3.2.1 Ear instance segmentation

To validate the effectiveness of the wheat ear instance segmentation method, the wheat ear point clouds obtained from organ segmentation of the same plant were clustered and segmented with different parameters ε. The segmentation results, where the same color represented the same category, are shown in Figure 12.

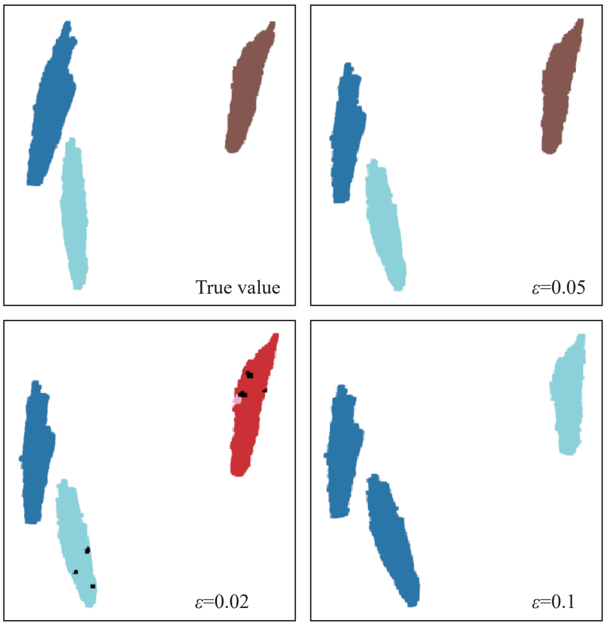

Figure 12 Results of wheat ear segmentation with different ε values

Additionally, 10 randomly selected wheat ear point clouds after organ segmentation were statistically segmented to verify the accuracy of the proposed wheat ear point cloud segmentation method. The results of counting the number of ears per wheat plant using manual annotation and clustering segmentation are listed in Table 2. Experimental results demonstrated that the segmentation method for ear instances achieved an average precision of 97%, average recall of 95%, and average F1 score of 96%. When the number of ears was high and they were densely packed and overlapping, segmentation failure primarily occurred.

3.2.2 Accurate registration based on the MVS algorithm

The visualization results of stem and leaf segmentation are shown in Figure 13, where different colors represent different organ instances. The accuracy assessment results of single wheat plant stem and leaf organ instance segmentation are presented in Table 3. From the table, it could be observed that the stem instance segmentation achieved average precision, recall, F1 score, and overall accuracy (OA) values of 0.909, 0.903, 0.906, and 0.923, respectively. The leaf instance segmentation achieved average precision, recall, F1 score, and OA values of 0.919, 0.914, 0.916, and 0.936, respectively. During the three-leaf stage, wheat plants exhibited a single stem structure, obviating the need for stem instance segmentation. These results demonstrated that the wheat stem and leaf instance segmentation method proposed in this chapter effectively segmented organ instances.

Table 2 Statistical results of wheat ear point cloud clustering and segmentation

No.	Precision	Recall	F1-score	Actual quantity	Cluster number
1	1.00	1.00	1.00	3	3
2	1.00	1.00	1.00	4	4
3	1.00	1.00	1.00	3	3
4	0.89	0.83	0.86	6	5
5	1.00	1.00	1.00	3	3
6	1.00	1.00	1.00	5	5
7	1.00	1.00	1.00	7	7
8	1.00	1.00	1.00	3	3
9	1.00	1.00	1.00	6	6
10	0.94	0.86	0.90	7	6

Table 3 Segmentation accuracy of stem and leaf point cloud instances at different growth stages

	Stem				Leaf			
	Precision	Recall	F1-score	OA	Precision	Recall	F1-score	OA
Trilobal stage	-	-	-	-	0.982	0.967	0.974	0.988
Tillering stage	0.924	0.908	0.916	0.941	0.875	0.881	0.878	0.893
Jointing- heading stage	0.893	0.897	0.895	0.905	0.901	0.894	0.897	0.926
Average value	0.909	0.903	0.906	0.923	0.919	0.914	0.916	0.936

3.3 Calculation and analysis of wheat phenotypic parameters

To evaluate the calculated phenotype parameters (plant height, plant compactness, ear width, ear length, ear volume, leaf length, leaf area, flag leaf inclination angle, leaf curvature, and stem inclination angle), we employed the coefficient of determination (R^2) and root mean square error (RMSE) to assess the goodness-of-fit and error levels against manual measurements. All experimental wheat phenotypes were measured during the manual measurement process. Specifically, plant height (from the tillering node to the ear tip, excluding awns), ear length (from the ear neck node to the ear tip, excluding awns), ear width (the widest part of the ear), and leaf length (from the leaf base to the leaf tip) were measured using a ruler. Flag leaf inclination angle (the angle between the flag leaf blade at its base, i.e., the leaf collar, and the stem) and stem inclination angle (the angle between the main stem base and the ground) were measured using a protractor. Ear volume was calculated as the product of the measured ear length, ear width, and ear thickness[44]. Leaf area was measured using the projection method: the leaf was flattened onto square grid paper with 1 cm^2 grids, its outline was traced, and the leaf area was determined by counting the number of grids covered.

The relationship between the algorithm-extracted wheat plant height values and manually measured values is shown in Figure 14a, indicating a strong correlation between the extracted and measured

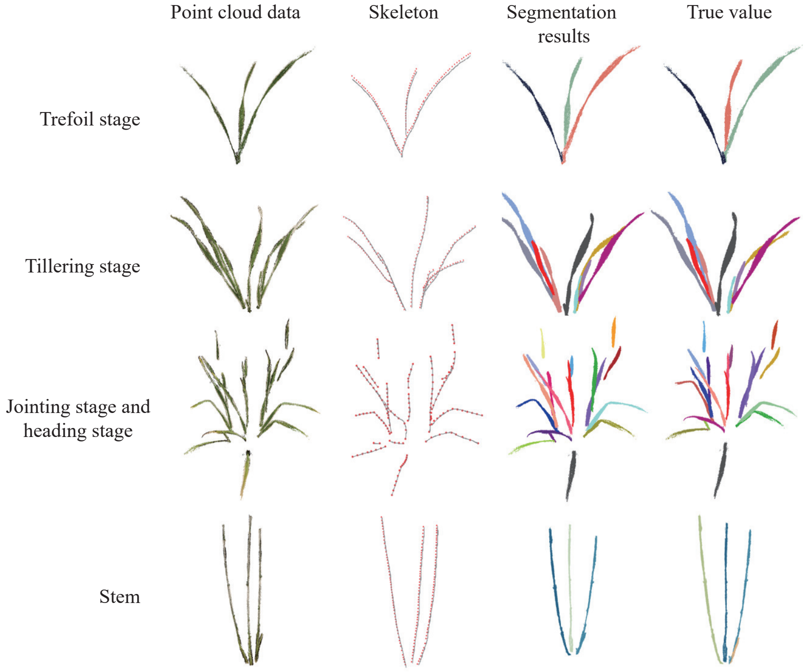

Figure 13 Results of wheat stalk and leaf point cloud example segmentation

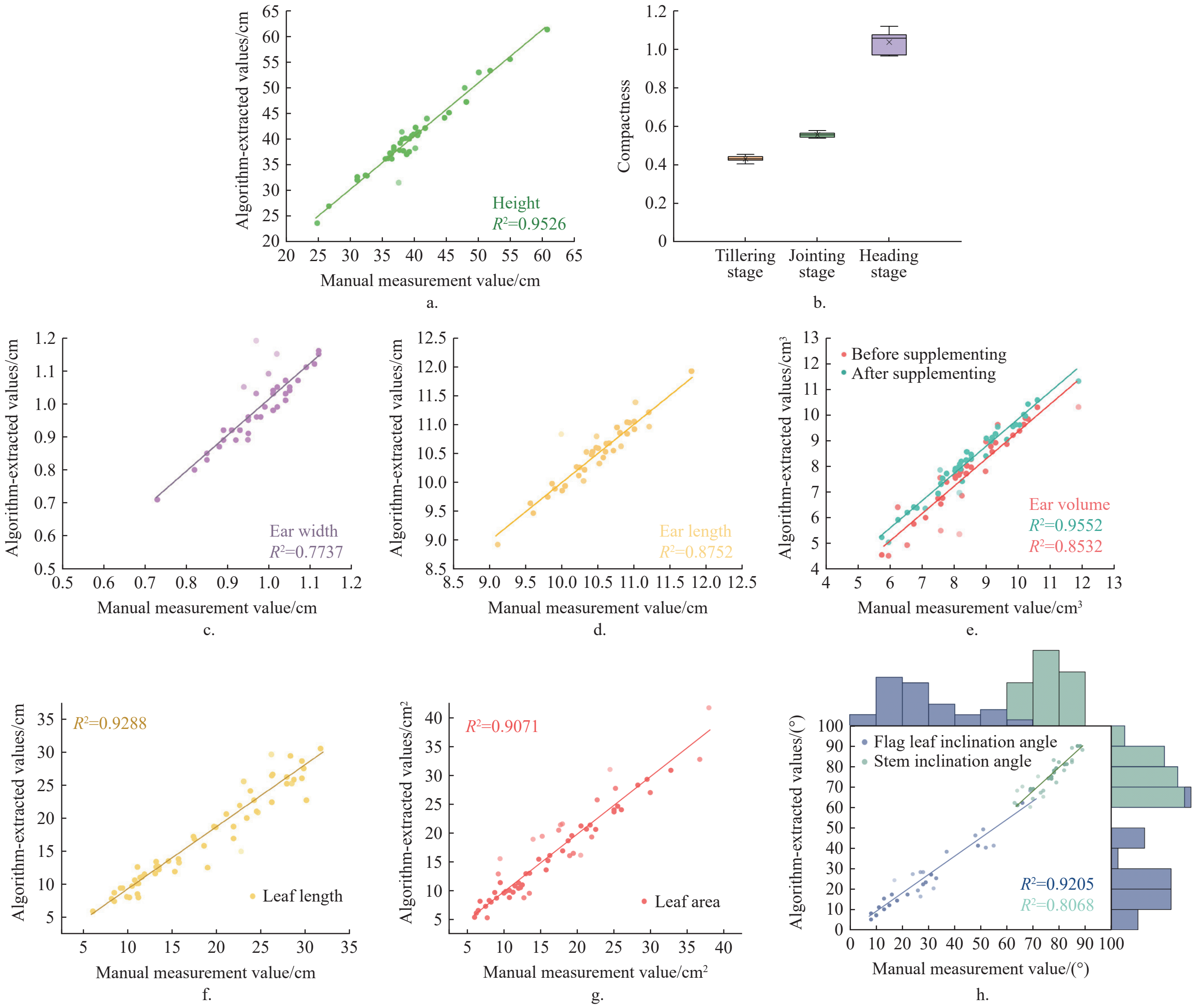

Figure 14 Comparison and correlation fitting results between extracted and manually measured values of wheat phenotypes

values. The coefficient of R^2 and RMSE were 0.9526 and 2.5490 cm, respectively. Wheat plant compactness during different growth stages is illustrated in Figure 14b. Compactness values ranged from 0 to 10, with wheat plants of the same growth stage having similar growth durations. The results indicated a correlation in compactness values among wheat plants at the same growth stage, and as wheat plants grew, their compactness increased gradually.

The relationship between automatically extracted values of three wheat ear phenotypes (ear length, ear width, ear volume) after organ segmentation and ear instance segmentation, compared to manually measured values, is shown in Figures 14c-14e and Table 4. Specifically, Figure 14e illustrates the volume changes of wheat ears before and after point cloud completion. After geometric symmetry-based point completion, the correlation between the extracted ear volume values and manually measured values strengthened, with an increase in the coefficient of R^2 by 0.1020 and in RMSE by 0.2756 cm^3.

Table 4 Results of correlation between extracted wheat phenotype values and manual measurements

	Height	Ear length	Ear width	Ear volume (before supplement point)	Ear volume (after supplement point)	Leaf length	Leaf area	Flag leaf inclination angle	Stem inclination angle
R^2	0.9526	0.8752	0.7737	0.8532	0.9552	0.9288	0.9071	0.9205	0.8068
RMSE	2.5490 cm	0.1951 cm	0.0520 cm	0.3710 cm^3	0.0954 cm^3	3.6037 cm	2.4128 cm^2	5.9048°	4.0083°

After organ segmentation and stem-leaf instance segmentation, the correlation between automatically extracted values of four wheat stem-leaf phenotypes (stem leaning degree, leaf length, flag leaf angle, leaf area) and manually measured values is shown in Figures 14f-14h. For leaf length, R^2 and RMSE were 0.9288 and 3.6037 cm, respectively. Leaf area achieved R^2 and RMSE values of 0.9071 and 2.4128 cm^2, respectively. For flag leaf inclination angle, R^2 and RMSE were 0.9205 and 5.9048°, respectively. Stem inclination angle exhibited R^2 and RMSE values of 0.8068 and 4.0083°, respectively. The results indicated a strong correlation between the algorithmically extracted values of these four phenotypic parameters and the manually measured values.

Figure 15 presents statistical results of leaf curvature for four different bending degrees. From the figure, it is evident that as the degree of leaf bending increased, the range of curvature fluctuation also gradually increased. Therefore, the average curvature fluctuation of the surface directly inferred the bending degree of wheat leaves.

4 Discussion

4.1 Construction of wheat dataset and organ classification

The proposed point-class-balance-based method for organ segmentation of wheat point clouds enables accurate segmentation of individual wheat organs at different growth stages. The balancing effect improves gradually as the patch size K decreases; however, an excessively small patch size fails to capture the global features of the organ point cloud, potentially leading to misclassification of point cloud categories by the network. When the patch size is set to K=2048, the differences in point proportions among categories become markedly smaller, and the segmentation accuracy for each organ tends to be balanced, achieving the best overall performance. This is primarily because the point clouds of wheat ears and stems exhibit a longitudinal distribution and contain relatively fewer points (approximately 10 000–60 000 for ears and 70 000–110 000 for stems at the heading stage), whereas leaf and non-plant point clouds are more uniformly distributed and much larger in size (approximately 160 000–300 000 for leaves and 180 000–300 000 for non-plant points at the heading stage). With K=2048, the method maximally preserves the point cloud information of ears and stems while reducing the numbers of leaf and non-plant points, thereby achieving class balance. Consequently, the proposed point-class-balance-based wheat organ segmentation method can automatically and accurately segment wheat organs at critical growth stages when the patch size is set to K=2048.

In addition, the proposed method was compared with commonly used semantic segmentation models, and the results demonstrate that RandLA-Net exhibits more balanced performance in the semantic segmentation of different wheat organs. It should be noted that, due to the limited sample size, whether RandLA-Net remains the optimal choice after further expansion of the dataset requires additional investigation. We will continue to acquire more wheat point cloud samples for such analyses. Furthermore, because the dataset used in this study was collected under controlled laboratory conditions, the wheat variety and data acquisition environment are relatively homogeneous. Although this study focuses primarily on the phenotyping of potted wheat plants under laboratory conditions, the practical need for organ-level phenotypic parameters in field breeding necessitates further exploration of the model's generalizability to complex field environments and to different wheat varieties (e.g., the multi-ear varieties Zhongmai 38 and Zhongmai 688). To this end, in future work, we will introduce mixed data augmentation strategies and point cloud spatial attention mechanisms to enhance the robustness of the model under more challenging scenarios.

4.2 Wheat organ instance segmentation and surface parameter acquisition

For instance segmentation of wheat organs, this study extracted point clouds of stems, leaves, and ears, respectively. For ear instance segmentation, a geometry-based point cloud completion strategy was proposed to effectively address the issue of missing ear points. Comparison with manually measured phenotypic traits (ear height, ear width, and ear volume) showed that after completion, the coefficient of determination (R^2) increased by 0.1020 and the root mean square error (RMSE) decreased by 0.2756 cm^3 compared to pre-completion values, validating the effectiveness of the proposed ear point cloud completion method. Residual errors in ear phenotype extraction mainly originate from two aspects. First, due to the specific structure of the ear—the Fielder wheat used in this study bears awns of considerable thickness—filtering cannot completely retain or remove the awn point cloud. Second, the manual measurement of ear volume approximates the volume as the product of ear length, width, and thickness; this method yields a slightly overestimated volume compared to the true value, with a deviation ranging from approximately 5% to 15%. It should be noted that the wheat plants in this experiment were grown under ideal laboratory conditions with relatively regular plant architecture. Even for curved or abnormal ears, the proposed completion algorithm maintains relatively high accuracy (with errors controlled within 10%–30%). Furthermore, owing to the resolution limitations of point cloud reconstruction, extremely fine structures such as

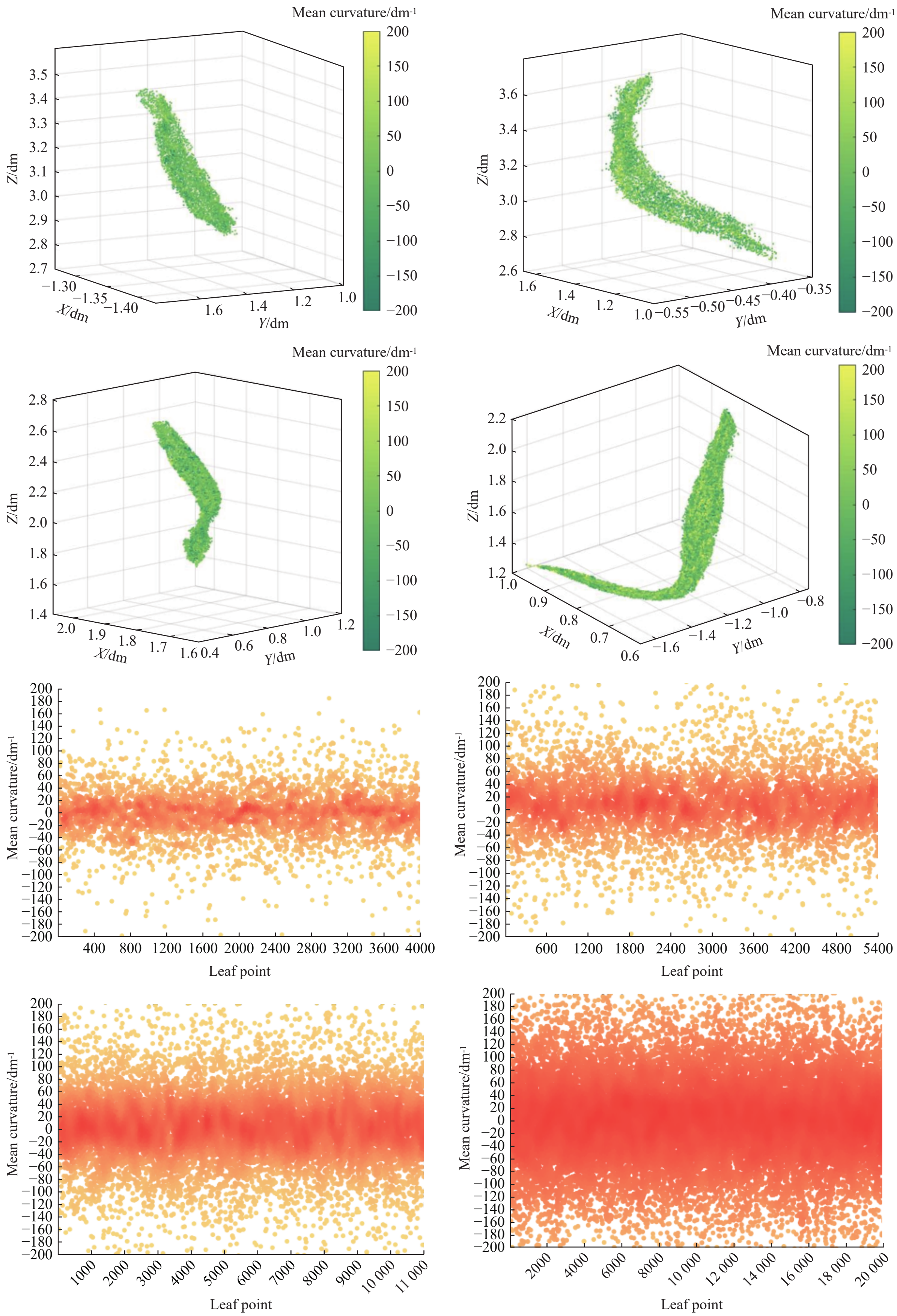

Figure 15 Visual results of leaf curvature comparison

awns were not included in the current phenotypic analysis; future studies may combine higher-precision scanning equipment for targeted investigations.

For stem and leaf instance segmentation, this study employed a skeleton extraction method based on the Laplace contraction operator. The overall segmentation accuracy exceeded 90%. Among all growth stages, the leaf point cloud instance segmentation results at the three-leaf stage showed the highest consistency with ground truth. Error analysis indicates that complete overlapping of leaf bases at the tillering stage is the primary cause of reduced segmentation accuracy during this period: the point clouds of adjacent leaves in the overlapping region are highly spatially overlapped, making it difficult for distance constraints to effectively assign each point to its correct leaf, thereby leading to misassignment of boundary points. After the jointing stage, the wheat stems elongate rapidly, causing the leaf bases to naturally separate and eliminating the overlapping interference; consequently, segmentation accuracy improves significantly. To address the errors caused by leaf base overlapping at the tillering stage, we suggest introducing curvature-based edge detection or fine-segmentation using local normal vector differences. For example, in addition to distance constraints, a leaf main-direction consistency constraint could be added to distinguish the basal point clouds of different leaves. Moreover, the stem characteristics of wheat show little variation across growth stages; mis-segmentation mainly occurs in the overlapping region between the short stems produced by secondary tillering and the base of the main stem. For this issue, an adaptive clustering method based on stem diameter or local point cloud density can be used to recognize and separate short stems as independent instances, thereby further improving the integrity of stem instance segmentation.

5 Conclusions

Organ-level phenotyping plays a vital role in crop breeding. In response to the need for intelligent and automated extraction of wheat phenotypic traits, this study introduces a method based on point cloud analysis for organ-level phenotyping during critical growth stages. First, multi-view images of potted wheat plants were acquired using a multi-view acquisition system. Using Structure from Motion (SfM) and Multi-View Stereo (MVS) methods, wheat point clouds were established, and a single-plant wheat point cloud segmentation dataset for key growth stages was constructed after preprocessing and point cloud annotation. Based on the structural characteristics of wheat plants, an organ semantic segmentation algorithm for wheat point clouds was proposed using class point balancing, resulting in an average overall accuracy (OA) and mean Intersection over Union (mIoU) improvement of 13.6% and 14.4%, respectively, compared to the unbalanced state. Additionally, considering the structure and location characteristics of each organ, a DBSCAN-based wheat ear instance segmentation algorithm using the maximum distance between *k*-nearest points and a stem-leaf instance segmentation method based on Laplacian contraction operator skeleton extraction were proposed. A geometric symmetry-based point completion method was designed to supplement wheat ear point clouds, addressing the partial loss of ear point clouds caused by filtering out awn point clouds. The results showed that the determination coefficient (R^2) between the supplemented ear volume extraction values and manual measurements improved by 10.2%, and the root mean square error (RMSE) decreased by 0.2756 cm^3. The correlation coefficients for ear length, ear width, and ear volume compared with manual measurements were 0.8752, 0.7737, and 0.9552, with RMSE values of 0.1951 cm, 0.0520 cm, and 0.0954 cm^3, respectively. The average OA and precision for wheat stem segmentation were 92.3% and 90.9%, respectively, while for leaf segmentation, they were 93.6% and 91.9%. The correlation coefficients for stem-leaf organ phenotypic measurements (stem inclination degree, leaf length, leaf area, and flag leaf angle) compared with manual measurements were 0.6739, 0.8068, 0.9288, and 0.9071, respectively. The wheat phenotyping extraction and measurement method designed in the study showed high consistency with actual results, providing a new, objective, and accurate method for obtaining phenotypic data, which is essential for screening and cultivating high-yield, stress-resistant new wheat varieties.

Acknowledgements

This research was supported by the Key R&D Program of Shandong Province, China (2022LZGCQY002; 2023TZXD004) and the ‘First Class Discipline’ Construction Project of Shandong Agricultural University (SKL81102). The authors are grateful to all study participants.

[References]

[1] Pieruschka R, Schurr U. Plant phenotyping: Past, present, and future. Plant Phenomics, 2019; 2019: 7507131.
[2] Tester M, Langridge P. Breeding technologies to increase crop production in a changing world. Science, 2010; 327(5967): 818–822.
[3] Reynolds M, Chapman S, Crespo-Herrera L, Molero G, Mondal S, Pequeno D N L, et al. Breeder friendly phenotyping. Plant Science, 2020; 295: 110396.
[4] Xiong J B, Yu D Z, Liu S Y, Shu L, Wang X C, Liu Z K. A review of plant phenotypic image recognition technology based on deep learning. Electronics, 2021; 10(1): 81.
[5] Lee U, Chang S Y, Putra G A, Kim H S, Kim D H. An automated, high-throughput plant phenotyping system using machine learning-based plant segmentation and image analysis. PloS one, 2018; 13(4): e0196615.
[6] Furbank R T, Tester M. Phenomics–technologies to relieve the phenotyping bottleneck. Trends in Plant Science, 2011; 16(12): 635–44.
[7] Liu Z C, Zhang Q, Wang P, Li Z, Wang H R. Automated classification of stems and leaves of potted plants based on point cloud data. Biosystems Engineering, 2020; 200: 215–30.
[8] Wang Y J, Wen W L, Wu S, Wang C Y, Yu Z T, Guo X Y, et al. Maize plant phenotyping: Comparing 3D laser scanning, multi-view stereo reconstruction, and 3D digitizing estimates. Remote Sensing, 2018; 11(1): 63.
[9] ElManawy A I, Sun D W, Abdalla A, Zhu Y M, Cen H Y. HSI-PP: A flexible open-source software for hyperspectral imaging-based plant phenotyping. Computers and Electronics in Agriculture, 2022; 200: 107248.
[10] Omari M K, Lee J Y, Faqeerzada M A, Joshi R, Park E S, Cho B-K. Digital image-based plant phenotyping: A review. Korean Journal of Agricultural Science, 2020; 47(1): 119–130.
[11] Das Choudhury S, Bashyam S, Qiu Y M, Samal A, Awada T. Holistic and component plant phenotyping using temporal image sequence. Plant Methods, 2018; 14(1): 1–21.
[12] Samant D, Dhawan R, Mishra A K, Bora V, Diwakar M, Singh P. Potato leaf disease detection using deep learning. In 2023 IEEE World Conference on Applied Intelligence and Computing (AIC), IEEE, 2023; pp.752–757.
[13] El-Sayed M E, Khodadadi N, Mirjalili S, Abdelhamid A A, Eid M M, Ibrahim A. Greylag goose optimization: Nature-inspired optimization algorithm. Expert Systems with Applications, 2024; 238: 122147.
[14] Das Choudhury S, Maturu S, Samal A, Stoerger V, Awada T. Leveraging image analysis to compute 3D plant phenotypes based on voxel-grid plant reconstruction. Frontiers in Plant Science, 2020; 11: 521431.
[15] Paulus S, Behmann J, Mahlein A-K, Plümer L, Kuhlmann H. Low-cost 3D systems: suitable tools for plant phenotyping. Sensors, 2014; 14(2): 3001–3018.
[16] Liu H, Xin C, Lai M Z, He H F, Wang Y Z, Wang M T, et al. RepC-MVSNet: A reparameterized self-supervised 3D reconstruction algorithm for wheat 3D reconstruction. Agronomy, 2023; 13(8): 1975.
[17] Sun S P, Li C Y, Paterson A H, Jiang Y, Xu R, Snider J L. In-field high throughput phenotyping and cotton plant growth analysis using LiDAR. Frontiers in Plant Science, 2018; 9: 315910.
[18] Gu Y Y, Wang Y Q, Wu Y P, Warner T A, Guo T, Ai H X, et al. Novel 3D photosynthetic traits derived from the fusion of UAV LiDAR point cloud and multispectral imagery in wheat. Remote Sensing of Environment, 2024; 311: 114244.
[19] Li Y F, Li C C, Cheng Q, Chen L, Li Z P, Zhai W G, et al. Precision

estimation of winter wheat crop height and above-ground biomass using unmanned aerial vehicle imagery and oblique photoghraphy point cloud data. Frontiers in Plant Science, 2024; 15: 1437350.

[20] Zou R, Zhang Y, Chen J, Li J Y, Dai W J, Mu S L. Density estimation method of mature wheat based on point cloud segmentation and clustering. Computers and Electronics in Agriculture, 2023; 205: 107626.

[21] Jagannathan A, Miller E L. Three-dimensional surface mesh segmentation using curvedness-based region growing approach. IEEE Transactions on Pattern Analysis and Machine Intelligence, 2007; 29(12): 2195–204.

[22] Ghahremani M, Williams K, Corke F M K, Tiddeman B, Liu Y H, Doonan J H. Deep segmentation of point clouds of wheat. Frontiers in Plant Science, 2021; 12: 608732.

[23] Duan T, Chapman S C, Holland E, Rebetzke G J, Guo Y, Zheng B. Dynamic quantification of canopy structure to characterize early plant vigour in wheat genotypes. Journal of Experimental Botany, 2016; 67(15): 4523–4534.

[24] Elnashef B, Filin S, Lati R N. Tensor-based classification and segmentation of three-dimensional point clouds for organ-level plant phenotyping and growth analysis. Computers and Electronics in Agriculture, 2019; 156: 51–61.

[25] Jin S C, Su Y J, Wu F F, Pang S X, Gao S, Hu T Y. Stem–leaf segmentation and phenotypic trait extraction of individual maize using terrestrial LiDAR data. IEEE Transactions on Geoscience and Remote Sensing, 2018; 57(3): 1336–1346.

[26] Wang D B, Song Z, Miao T, Zhu C, Yang X, Yang T, et al. DFSP: A fast and automatic distance field-based stem-leaf segmentation pipeline for point cloud of maize shoot. Frontiers in Plant Science, 2023; 14: 1109314.

[27] Zhou J, Fu X Q, Zhou S Q, Zhou J F, Ye H, Nguyen H T. Automated segmentation of soybean plants from 3D point cloud using machine learning. Computers and Electronics in Agriculture, 2019; 162: 143–153.

[28] Ge X F, Wu S, Wen W L, Shen F, Xiao P L, Lu X J, et al. LettuceP3D: A tool for analysing 3D phenotypes of individual lettuce plants. Biosystems Engineering, 2025; 251: 73–88.

[29] Griffiths D, Boehm J. A review on deep learning techniques for 3D sensed data classification. Remote Sensing, 2019; 11(12): 1499.

[30] Jin S C, Su Y J, Gao S, Wu F F, Ma Q, Xu K X, et al. Separating the structural components of maize for field phenotyping using terrestrial LiDAR data and deep convolutional neural networks. IEEE Transactions on Geoscience and Remote Sensing, 2019; 58(4): 2644–2658.

[31] Patel A K, Park E-S, Lee H S, Lakshmi Priya G G, Kim H, Joshi R, et al. Deep learning-based plant organ segmentation and phenotyping of sorghum plants using LiDAR point cloud. IEEE Journal of Selected Topics in Applied Earth Observations and Remote Sensing, 2023; 16: 8492–8507.

[32] Gong L, Du X F, Zhu K, Lin K, Lou Q J, Yuan Z, et al. Panicle-3D: efficient phenotyping tool for precise semantic segmentation of rice panicle point cloud. Plant Phenomics, 2021; 2021: 9838929.

[33] Li Y L, Wen W L, Miao T, Wu S, Yu Z T, Wang X D, et al. Automatic organ-level point cloud segmentation of maize shoots by integrating high-throughput data acquisition and deep learning. Computers and Electronics in Agriculture, 2022; 193: 106702.

[34] Xiao P L, Wu S, Gao S Q, Wen W L, Wang C Y, Lu X J, et al. ICFMNet: an automated segmentation and 3D phenotypic analysis pipeline for plant, spike, and flag leaf type of wheat. Computers and Electronics in Agriculture, 2025; 239: 110893.

[35] Zhang J Y, Zhao X L, Chen Z, Lu Z J. A review of deep learning-based semantic segmentation for point cloud. IEEE Access, 2019; 7: 179118–179133.

[36] Hu Q Y, Yang B, Xie L H, Rosa S, Guo Y L, Wang Z H, et al. Randla-net: Efficient semantic segmentation of large-scale point clouds. In Proceedings of the IEEE/CVF Conference on Computer Vision and Pattern Recognition, 2020; pp.11108–11117. DOI: 10.1109/CVPR42600.2020.01112

[37] Boogaard F P, Van Henten E J, Kootstra G. Improved point-cloud segmentation for plant phenotyping through class-dependent sampling of training data to battle class imbalance. Frontiers in Plant Science, 2022; 13: 838190.

[38] Liu Y Y, Chen J, Yin C B, Wang Z Y, Wu H, Shen K C, et al. A high-resolution genotype–phenotype map identifies the TaSPL17 controlling grain number and size in wheat. Genome Biology, 2023; 24(1): 196.

[39] Fang J J, Guo T T, Xie Z W, Chun Y, Zhao J F, Peng L X, et al. The URL1–ROC5–TPL2 transcriptional repressor complex represses the ACL1 gene to modulate leaf rolling in rice. Plant Physiology, 2021; 185(4): 1722–1744.

[40] Monti F, Boscaini D, Masci J, Rodola E, Svoboda J, Bronstein M M. Geometric deep learning on graphs and manifolds using mixture model CNNS. In Proceedings of the IEEE Conference on Computer Vision and Pattern Recognition, 2017; pp.5115–5124.

[41] Li Y Y, Bu R, Sun M C, Wu W, Di X H, Chen B Q. Pointcnn: Convolution on X-transformed points. Advances in Neural Information Processing Systems, 2018; 31: 450.

[42] Hugues T, Charles R Q, Deschaud J E, Marcotegui B, Goulette F, Guibas L J. KPConv: Flexible and deformable convolution for point clouds. In Proceedings of the IEEE/CVF International Conference on Computer Vision, 2019; pp.6411–6420.

[43] Verma N, Boyer E, Verbeek J. Feastnet: Feature-steered graph convolutions for 3d shape analysis. In Proceedings of the IEEE Conference on Computer Vision and Pattern Recognition, 2018; pp.2598–2606.

[44] Wang F L, Li F P, Mohan V, Dudley R, Gu D B, Bryant R. An unsupervised automatic measurement of wheat spike dimensions in dense 3D point clouds for field application. Biosystems Engineering, 2022; 223: 103–114.